

Impact of Hysteresis curve on subthreshold swing in ferroelectric FET

Hakkee Jung

Department of Electronic Eng., Kunsan National University, Gunsan, South Korea 54150

*Emails: hkjung@kunsan.ac.kr

Received: 7 August 2023; Accepted for publication: 15 December 2023

Abstract. The changes in Subthreshold Swing (SS) were observed for changes in remanent polarization P_r and coercive field E_c , which determine the characteristics of the P - E hysteresis curve of ferroelectric in Ferroelectric FET (FeFET). A Metal-Ferroelectric-Metal-Insulator-Semiconductor (MF MIS) structure was used for the junctionless double gate structure. To obtain the SS value, the analytical SS model was used. The ranges of $15 \leq P_r \leq 30 \mu\text{C}/\text{cm}^2$ and $0.8 \leq E_c \leq 1.5 \text{ MV}/\text{cm}$, which were reasonable in various experiments and did not generate unstable regions in the relationship of drain current and gate voltage, were considered. As a result, the SS decreased as P_r decreased and E_c increased due to the capacitance change in the ferroelectric. This phenomenon is because the controllability of channel carriers by the gate voltage increases due to the increasing of change in the ferroelectric voltage for the gate voltage as P_r decreases and the memory window increases. Since the SS decreased linearly in the memory window, the SS constantly changed according to the ratio of P_r and E_c , P_r/E_c . As the ferroelectric thickness increased, the SS decreased significantly, but the change of SS for the P_r/E_c was severe. In general, as the channel length decreases, SS increases. However, when the P_r/E_c decreased to $10 \text{ pF}/\text{cm}$, the SS tended to decrease as the channel length decreased. The reason for this can be attributed to the fact that the relative thickness of ferroelectric increases with a small channel length.

Keywords: subthreshold swing, junctionless, ferroelectric, remanent polarization, coercive field.

Classification numbers: 2.2.2, 2.4.1, 4.1.1.

1. INTRODUCTION

High integration is a very necessary factor not only for economic reasons such as reduction in production cost but also for engineering aspects such as applications in the ultra-high frequency region by high-speed switching operations due to reduced transistor sizes. Therefore, reducing the size of the transistor is a key matter, but it becomes an obstacle to high integration because of the increase of short-channel effect that affects the increase in power consumption, such as the increase in subthreshold swing (SS) or the increase in off-current caused by the decrease in transistor size [1 - 3]. As a result, the decrease in transistor size represents the disadvantage of increased power consumption as well as the advantage of high-speed operation. To solve this problem, the structure of the transistor is being changed three-dimensionally, such

as FinFET or GAA FET, and the gate oxide material is made of high- k dielectric stacked with SiO₂ or the hysteresis characteristics of ferroelectric materials are being used [4 - 6]. Among them, FETs using ferroelectric show an SS of less than 60 mV/dec and are in the spotlight as devices for low power consumption [7 - 9]. Since the decrease in SS eventually appears as a decrease in parasitic current, the decrease in SS is a very important factor in miniaturizing transistors. However, Boltzmann Tyranny limited the SS value to a minimum value of 60 mV/dec. Even when high- k was used in the already announced junctionless double-gate MOSFET and GAA FET [10 - 11], it was confirmed that SS > 60 mV/dec if the negative capacitance effect of ferroelectric was not used. Several papers have already been published showing SS values below 60mV/dec using the Ferroelectric FET (FeFET) to overcome these difficulties [12 - 14].

In particular, HfO₂-based ferroelectric devices are being studied extensively due to their integration, low power consumption, and excellent compatibility with CMOS technology. Therefore, in this paper, the change of SS according to the hysteresis characteristics of HfZrO (HZO) in HfO₂-based ferroelectric FET (FeFET) is analyzed. The P - E curve, which shows the relationship between ferroelectric polarization and electric field, exhibits hysteresis characteristics and varies greatly depending on the manufacturing process of the ferroelectric material [15 - 17].

Since the shape of the P - E curve greatly affects the SS of FeFET, research on the P - E hysteresis curve of ferroelectric is being actively conducted. Das *et al.* presented the change of composition of Hf and Zr and the transition of the P - E curve according to the heat treatment using Rapid Thermal Annealing (RTA) for the ferroelectric layer having the same composition [18 - 19]. Chen and Yuan *et al.* analyzed the effect of NH₃ plasma treatment on reliability during TiN/HZO/TiN formation using the P - E curve, and Dang *et al.* also studied the endurance of HZO-based ferroelectric capacitor according to the Ti to N ratio during TiN electrode formation [20 - 22]. The two variables that determine the shape of the P - E curve are the remanent polarization P_r and the coercive field E_c . As the P_r and E_c modify the capacitance of the ferroelectric, the two factors have a significant impact on the SS [23 - 24]. In addition, since P_r and E_c affect leakage current, wake-up, cycling endurance, and retention of ferroelectric devices, they have a great influence on the electrical characteristics of FeFET using ferroelectric thin film [25 - 27]. Therefore, in this paper, the effect of changes in P_r and E_c on the SS of FeFET having a Metal-Ferroelectric-Metal-Insulator-Semiconductor (MF MIS) structure is investigated. A particular focus will be placed on junctionless double-gate FeFETs. Further, the potential of junctionless double-gate FeFETs for integrated circuit applications will be investigated.

2. THEORETICAL BACKGROUND

2.1. The hysteresis of ferroelectric and FeFET

Figure 1 shows the transition of the P - E hysteresis curve of ferroelectric for the change of remanent polarization P_r and coercive field E_c . As seen from Figure 1, the absolute value of the negative capacitance of a ferroelectric material can be expressed as the rate of change of polarization P for electric field E . Figure 1(a) is a picture of changing E_c after fixing P_r . As seen in Figure 1(a), as E_c decreases, the absolute value of negative capacitance increases. Also, in Figure 1(b), it can be seen that the absolute value of negative capacitance increases when E_c is fixed and P_r is increased. In this way, when the P_r and E_c change, it can be found that the value of negative capacitance changes due to the change of the hysteresis curve of the ferroelectric.

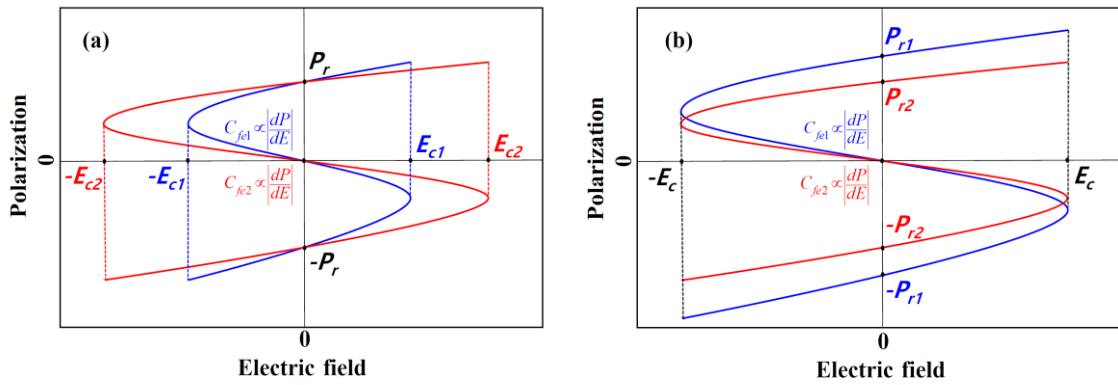


Figure 1. The change of the P - E hysteresis curve and the change of the corresponding capacitance for the change of P_r and E_c .

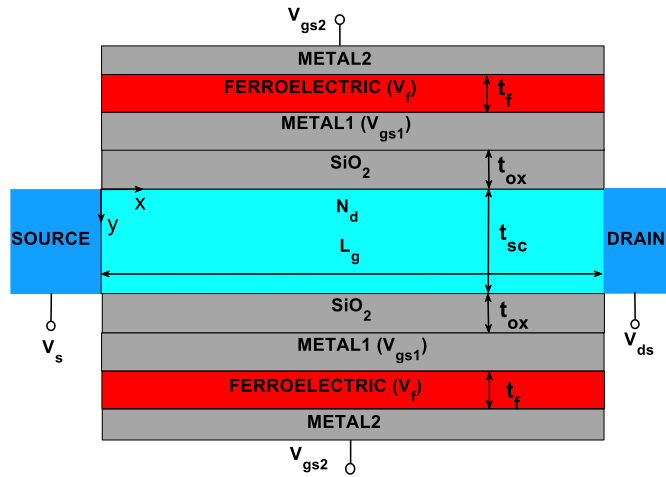


Figure 2. Schematic overview of a junctionless double gate FeFET with MF MIS structure.

Table 1. Device parameters for this analytical threshold voltage model.

| Device parameter | Symbol | Value |
|----------------------------|----------|-----------------------------------|
| Channel length | L_g | 15 ~ 40 nm |
| Channel width | W | 1 μ m |
| Channel thickness | t_{sc} | 10 nm |
| SiO ₂ thickness | t_{ox} | 1 ~ 2 nm |
| Doping concentration | N_d | 10 ¹⁹ /cm ³ |
| Ferroelectric thickness | t_f | 1 ~ 15 nm |
| Remanent polarization | P_r | 15 ~ 30 μ C/cm ² |
| Coercive field | E_c | 0.8 ~ 1.5 MV/cm |

Figure 2 shows the FeFET with the junctionless double gate of the MFMS structure used in this paper. The symbols shown in Figure 2 and the range of device parameters used in this paper are shown in Table 1.

2.2. P_r and E_c values used in a simulation

The P_r and E_c values vary according to various experiments. Figure 3 shows the P_r and E_c values corresponding to HZO ferroelectric extracted from published papers [18 - 21, 28 - 30]. As seen in Figure 3, it can be found that the P_r and E_c values are very diverse depending on the experimental conditions or the ratio of Hf and Zr. Therefore, we will observe the change of SS in the range of P_r and E_c corresponding to the box value indicated by the dotted line where most of the experimental values are gathered in Figure 3.

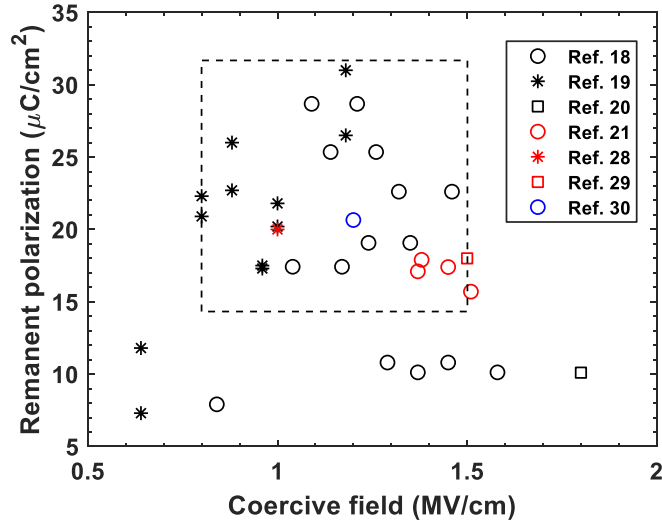


Figure 3. Material parameters of ferroelectric HZO thin films published in previous papers.

3. RESULTS AND DISCUSSIONS

3.1. The Change of SS and I-V Curves for P_r and E_c

Ding's expansion method [31] was used to obtain the potential distribution within the channel for the MFMS FeFET shown in Figure 2, and the current-voltage characteristics were obtained using the expansion method presented in the previous paper [32]. The swing was obtained using $dV_{gs2}/d\log(I_{ds})$ by the definition of SS with drain current I_{ds} and gate voltage V_{gs2} to find out the change of swing in the subthreshold region. First, after fixing $E_c = 1$ MV/cm in Figure 4, the drain current-gate voltage characteristics and swing obtained with P_r as a parameter are shown. As seen in Figure 4(a), as P_r increases under the given conditions, the current level decreases and the subthreshold current decreases more rapidly. In addition, it can be observed that the on-current is almost unaffected by P_r , but the off-current rapidly decreases as P_r increases. Figure 4(b) shows the swing values obtained by calculating the value of $dV_{gs2}/d\log(I_{ds})$ in current-voltage curves of Figure 4(a). It can be observed that the subthreshold swing decreases as the P_r value increases in the subthreshold region with a sufficiently small drain current. In particular, it can be observed that the SS is less than 60 mV/dec in the case of $P_r = 30$ $\mu\text{C}/\text{cm}^2$ under the given conditions.

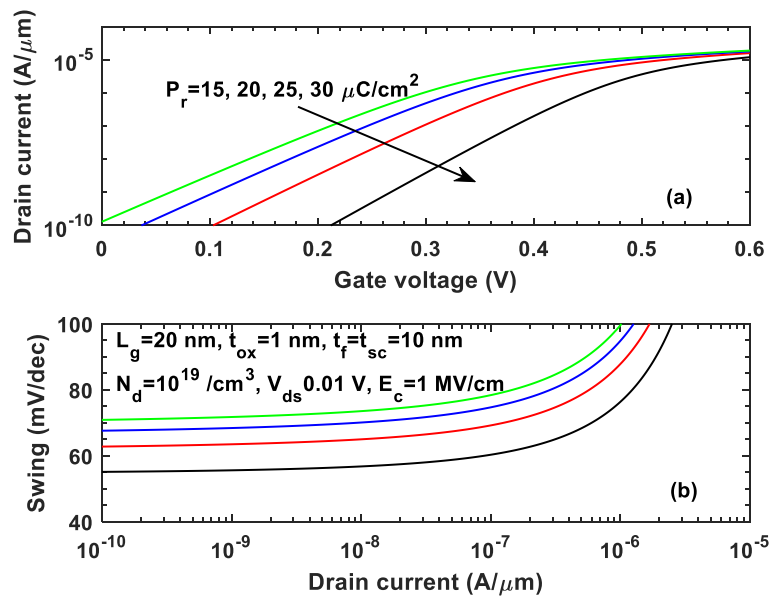


Figure 4. (a) The relationship of drain current vs. gate voltage (V_{gs2} in Figure 2), and (b) swings defined by $dV_{gs2}/d\log(I_{ds})$ with the remanent polarization as a parameter under the conditions shown in the figure.

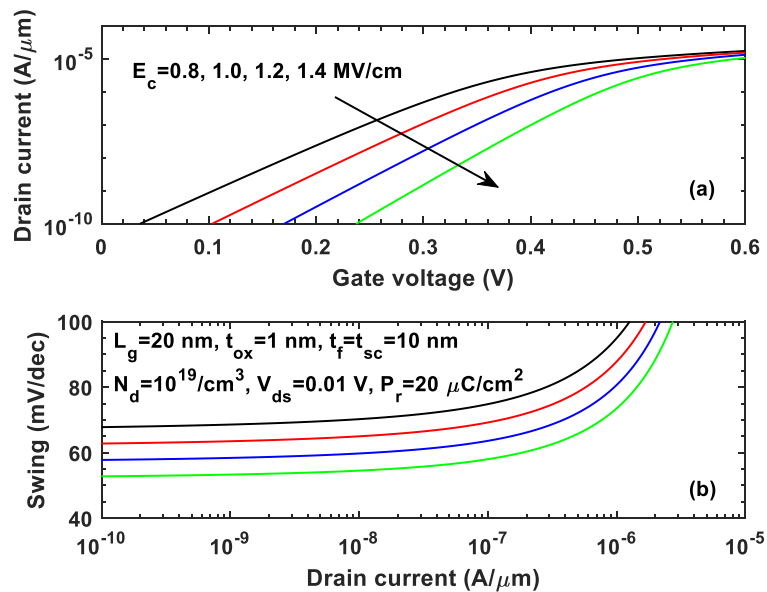


Figure 5. (a) The relationship of drain current vs. gate voltage (V_{gs2} in Figure 2), (b) swings defined by $dV_{gs2}/d\log(I_{ds})$ with the coercive field as a parameter under the conditions shown in the figure.

Figure 5 shows the drain current-gate voltage characteristics and swing obtained in the same way as Figure 4 with P_r fixed at $20 \mu C/cm^2$ and E_c as a parameter. Observing Figure 5(a), it can be seen that the current level decreases as E_c increases, and in particular, the off-current decreases rapidly. As shown in Figure 5(b), when E_c increases, the threshold voltage increases even though the off-current and threshold voltage have a

large effect on power consumption. Figure 5(b) shows the swing value obtained in the same way as in Figure 4(b). As E_c increases, the swing value decreases, and it can be observed that SS is less than 60 mV/dec when $E_c = 1.2$ MV/cm and $E_c = 1.4$ MV/cm in the subthreshold region under the given conditions. As mentioned above, since the SS changed greatly with the change of P_r and E_c , this paper will focus on the change of SS for P_r and E_c .

Next, the relationship between SS and ferroelectric capacitance C_{fe} is explained with the P - E relationship in Figure 1. For the FeFET of the MFMIS structure shown in Figure 2, the relationship between SS and the absolute value of ferroelectric capacitance C_{fe} presented by Tu *et al.* is as shown in Eq. (1) [16].

$$SS = \left(1 + \frac{C_s}{C_{ox}}\right) \left(1 - \frac{C_{MIS}}{|C_{fe}|}\right) \times 60 \text{ [mV / dec]} \quad (1)$$

here, C_s is the capacitance of the semiconductor, C_{ox} is the capacitance of the oxide used as the insulator layer. C_{MIS} is the capacitance corresponding to the MISFET (Metal Insulator Semiconductor FET) in the MFMIS FET structure and corresponds to the value of $(1/C_{ox}+1/C_s)^{-1}$. In this paper, since we want to examine the change of SS for the P - E curve of ferroelectric, we will eventually examine the change of SS for the change of $|C_{fe}|$. As seen from Eq. (1), SS decreases when $|C_{fe}|$ decreases, and SS also increases when $|C_{fe}|$ increases. As described above, since $|C_{fe}|$ is determined according to P_r and E_c values, the SS is determined according to P_r and E_c .

3.2. Subthreshold swing of FeFET

First, to obtain the SS for the changes in P_r and E_c , an analytical SS model derived from Ding's extension method [31] was used, as in Eq. (2), which was already verified in a published paper [31].

$$SS = \frac{\partial V_{gs2}}{\partial \log I_{ds}} = \ln(10) \left(\frac{kT}{q} \right) \left(\frac{\partial \phi_{\min}}{\partial V_{gs2}} \right)^{-1} \quad (2)$$

$$\frac{\partial \phi_{\min}}{\partial V_{gs2}} = \sum_{n=1}^{\infty} \frac{\partial A_n(y)}{\partial V_{gs2}} \sin \left(\frac{n\pi x}{L_g} \right) \Bigg|_{x=x_{\min}, y=t_{sc}/2} = \sum_{n=1}^{\infty} \frac{\partial A_n(t_{sc}/2)}{\partial V_{gs2}} \sin \left(\frac{n\pi x_{\min}}{L_g} \right)$$

$$\frac{\partial A_n(t_{sc}/2)}{\partial V_{gs2}} = \frac{2e^{k_n t_{sc}/2} C_{ox} \left(\frac{2}{n\pi} [1 - (-1)^n] \right)}{\left[e^{k_n t_{sc}} (C_{ox} + \varepsilon_{si} k_n) + (C_{ox} - \varepsilon_{si} k_n) \right]} \times$$

$$\frac{1}{C_{ox} \left\{ 1 + \sum_{n=1}^{\infty} \frac{\partial C_n}{\partial V_{gs1}} \left(1 + e^{k_n t_{sc}} \right) \left(\frac{1}{n\pi} \right) [(-1)^n - 1] \right\}} \times$$

$$\frac{1}{2\alpha t_f + 12\beta t_f Q^2 + 30\gamma t_f Q^4 + \frac{\partial V_{gs1}}{\partial Q}}$$

$$\frac{\partial V_{gs1}}{\partial Q} = \frac{1}{C_{ox} + \sum_{n=1}^{\infty} \frac{\partial C_n}{\partial V_{gs1}} (1 + e^{k_n t_{sc}}) \left(\frac{1}{n\pi} \right) [(-1)^n - 1]}$$

$$\frac{\partial C_n}{\partial V_{gs1}} = \frac{C_{ox} \left(\frac{2}{n\pi} [1 - (-1)^n] \right)}{\left[e^{k_n t_{sc}} (C_{ox} + \varepsilon_{si} k_n) + (C_{ox} - \varepsilon_{si} k_n) \right]},$$

$$k_n = \frac{n\pi}{L_g}, \quad \alpha = -\frac{3\sqrt{3}}{2} \frac{E_c}{P_r} (m/F), \quad \beta = \frac{3\sqrt{3}}{2} \frac{E_c}{P_r^3} (m^5/F/C^2), \quad \gamma = 0$$

here, C_{ox} is the oxide film capacitance, ε_{si} is the dielectric constant of silicon, and Q is the ferroelectric charge, as described in the previous paper [32].

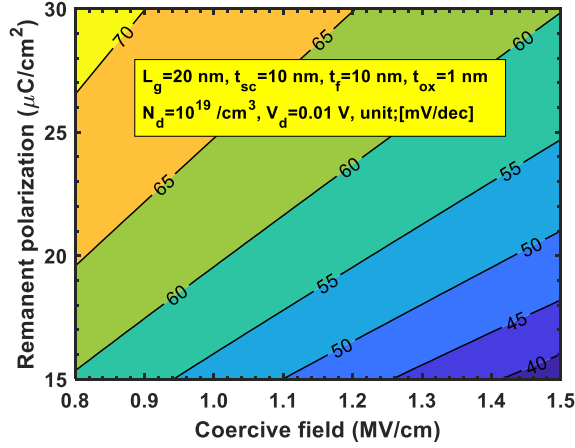


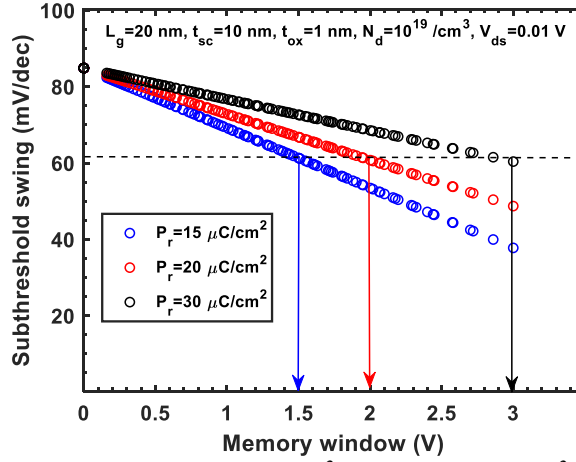
Figure 6. Contour plot for remanent polarization and coercive field under the conditions presented in the figure.

The value of the SS obtained using the analytical subthreshold swing model is shown in Figure 6 as a contour plot for P_r and E_c . As described above, the SS increases as P_r increases, and decreases as E_c increases. Of course, both P_r and E_c have a non-monotonic relationship with the SS due to the polarization effect [33], and it can be seen that SS decreases when E_c increases in the region where P_r is $15 \mu\text{C}/\text{cm}^2$ or more. In particular, the SS values of 60 mV/dec or less were shown in almost half of the simulation area.

Observing Figure 6, it can be seen that P_r and E_c must increase simultaneously to maintain a constant SS value. In addition, it can be observed that the SS is almost similar when the ratio of P_r to E_c is the same. This is because the capacitance C_{fe} of ferroelectric is proportional to $|dP/dE|$ as described in Figure 1, and eventually the SS will change according to C_{fe} in Eq. (1) if all conditions are the same.

To examine this relationship in more detail, the relationship between the memory window expressed as $2t_f E_c$ and the SS is shown in Figure 7 with P_r as a parameter. The simulation ranges are $0 \leq t_f \leq 10 \text{ nm}$, $15 \leq P_r \leq 30 \mu\text{C}/\text{cm}^2$ and $0.8 \leq E_c \leq 1.5 \text{ MV}/\text{cm}$, and the given conditions are indicated in the figure. As shown in Figure 7, the SS decreases as the memory window increases, and the degree of decrease reduces as P_r increases. That is, when P_r increases, the SS

increases, but it can be seen that the dependence on the memory window decreases. As mentioned in Figure 6, if the ratio of memory window and P_r is the same, the SS shows almost the same value. That is, when the memory window is 1.5 V at $P_r = 15 \mu\text{C}/\text{cm}^2$, the SS value of about 61 mV/dec is shown, and it can be observed that the same SS value is shown even when



the memory window is 2 V and 3 V at $P_r = 20 \mu\text{C}/\text{cm}^2$ and $P_r = 30 \mu\text{C}/\text{cm}^2$, respectively.

Figure 7. Relationships of subthreshold swing and memory window ($= 2t_f E_c$) with a remanent polarization as a parameter under the conditions given in the figure.

As seen in Figures. 6 and 7, it can be seen that the SS decreases as P_r decreases and the memory window increases. The decrease in SS means that the ability to control the channel carrier by the gate voltage increases. To examine these matters in greater detail, the change of the voltage V_{gs1} of METAL1 and the voltage V_f of ferroelectric according to the voltage applied at METAL2 in Figure 2 is shown for the remanent polarization with the memory window as a parameter in Figure 8. A large dV_{gs1}/dV_{gs2} means that a small change in V_{gs2} causes a large change in V_{gs1} . Here, since V_{gs1} directly affects the drain current, the drain current will also change significantly and the SS will decrease accordingly when dV_{gs1}/dV_{gs2} increases. In Figure 8, it can be seen that the smaller P_r and the larger memory window increase dV_{gs1}/dV_{gs2} , which is also explained in Figure 7. Figure 8 shows how the voltage applied to the ferroelectric changes according to V_{gs2} . In Figure 2, since the voltage across METAL2 is $V_{gs2} = V_{gs1} + V_f$, it can be observed that the relationship is like $dV_f/dV_{gs2} = 1 - dV_{gs1}/dV_{gs2}$. Therefore, it shows the opposite relationship with dV_{gs1}/dV_{gs2} in Figure 8. As P_r decreases and the memory window increases, it can be seen that the voltage V_f across the ferroelectric greatly varies according to V_{gs2} . If V_f greatly varies according to V_{gs2} , it means that the drain current can be greatly changed according to V_{gs2} , that is, the controllability of carriers in the channel by V_{gs2} is improved, so the SS will decrease. Comparing Figure 7 and Figure 8, it can be seen that the change in P_r and memory window is an important factor in determining the degree of change in drain current by V_{gs2} .

As mentioned in Figure 6 and Figure 7, if the ratio of P_r and E_c is the same, the SS is almost the same. The characteristic of HZO film is that it shows excellent ferroelectricity even at several nm [34 - 35]. Therefore, we tried to observe the change of SS according to the ratio of P_r and E_c using the ferroelectric thickness t_f as a parameter, and the result is shown in Figure 9. The SS were calculated for the range of the P_r and E_c shown in Table 1, and the given conditions are

indicated in Figure 9. As shown in Figure 9, the SS decreases significantly when the ferroelectric thickness becomes thicker.

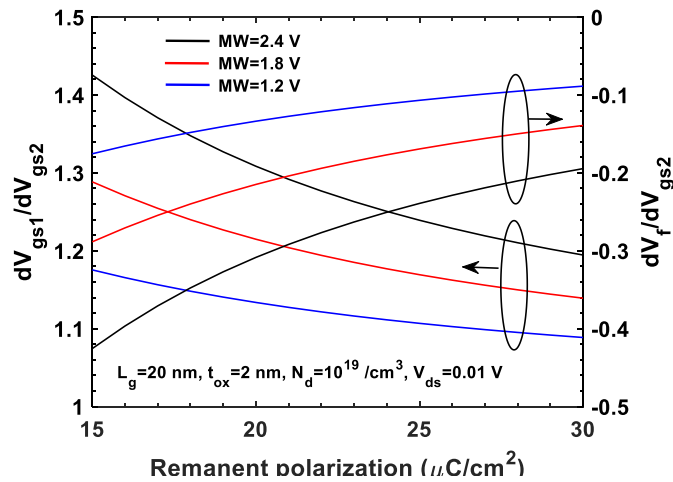


Figure 8. Changes in voltage V_{gs1} across METAL1 and voltage V_f across ferroelectric for changes in voltage V_{gs2} across METAL2 with the remanent polarization and memory window as parameters under the conditions given in the figure.

However, as the ferroelectric thickness becomes thinner, the SS increases and the change of the SS for the change of the ratio of remanent polarization P_r and coercive field E_c also decreases. That is, it can be observed that the SS is hardly affected by the ratio of remanent polarization and coercive field when the ferroelectric thickness becomes smaller. This is because the effect of ferroelectricity decreases as the thickness decreases. Looking at Figure 9, it can be seen that the SS is saturated when the ratio of remanent polarization and coercive field is above the critical value. Also, as the ratio of remanent polarization and coercive field decreases, the SS changes greatly according to ferroelectric thickness. However, as the ratio of remanent polarization and coercive field increases, it can be observed that the variation of SS according to ferroelectric thickness decreases.

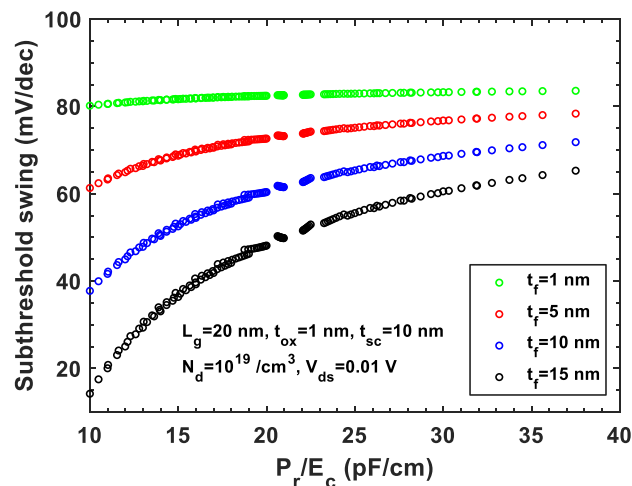
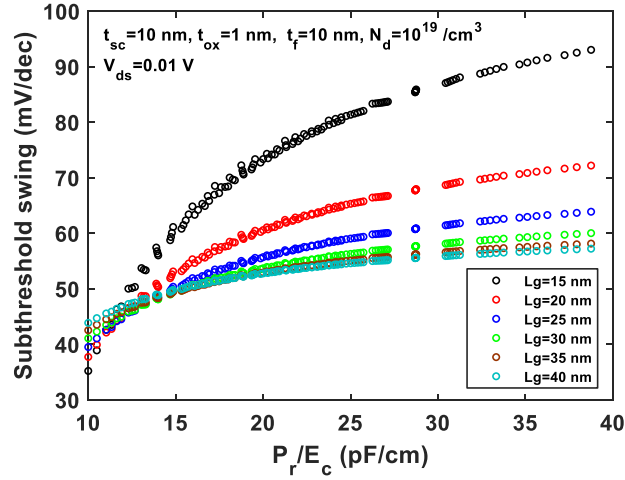


Figure 9. Subthreshold swings for the ratio of remanent polarization and coercive field with a ferroelectric thickness as a parameter under the conditions given in the figure.

To find out how the P_r/E_c of ferroelectric affects the current-voltage characteristics according to the channel length of FeFET, the relationship between drain current and gate voltage is shown in Figure 10 when the P_r/E_c is 10 pF/cm and 30 pF/cm. As described above, it can be observed in Figure 10 that the SS increases as P_r/E_c increases. In addition, it can be seen that the SS increases rapidly when the channel length decreases with P_r/E_c being as large as 30 pF/cm. However, when P_r/E_c is relatively small, it can be observed that the SS decreases further as the channel length decreases. As seen in Figure 1, a small P_r/E_c means a small C_{fe} , and at this time, it can be observed that the change of the P - E curve becomes more severe. That is, strong ferroelectricity occurs and SS decreases. In particular, as the channel length becomes shorter, the ferroelectric thickness increases relatively, so the ferroelectricity also increases and the SS will further decrease. Note that $SS > 60$ mV/dec when $P_r/E_c = 30$ pF/cm and $SS < 60$ mV/dec when



$P_r/E_c = 10$ pF/cm. In addition, as P_r/E_c decreases, an unstable region appears as shown in the red dotted line in Figure 10, so in this paper, simulations were performed in the range of $P_r/E_c > 10$ pF/cm.

Figure 10. Relation of drain current and gate voltage with the ratio of remanent polarization P_r and coercive field E_c and channel length as parameters under the conditions given in the figure.

Based on the characteristics of Figure 10, the change of SS according to P_r/E_c is shown in Figure 11 with the channel length as a parameter. As mentioned in Figure 10, when P_r/E_c decreases, it can be seen that SS decreases as C_{fe} decreases. The degree of change of SS according to P_r/E_c increased as the channel length decreased, and as the channel length increased, the change rate of SS according to P_r/E_c also decreased due to the relative decrease in ferroelectric thickness. In addition, as P_r/E_c increases, the change of SS according to the channel length increases, and as P_r/E_c decreases, the change of SS according to the channel length decreases. In particular, for the reason explained in Figure 10, it can be seen that SS decreases as the channel length decreases with P_r/E_c being around 10 pF/cm. The ranges of P_r and E_c indicated in Table 1 were limited to ranges where unstable regions did not appear in the relationship between drain current and gate voltage, if possible. The curvature of the hysteresis curve increases when P_r becomes smaller than E_c and P_r/E_c becomes smaller. An unstable region begins to appear in the current-voltage characteristic as shown in Figure 10, and SS rapidly decreases.

Figures 9 and 11 show the relationship between P_r/E_c , channel length, and ferroelectric

thickness to maintain the SS value below 60 mV/dec. To find the range of these parameters to satisfy $SS < 60$ mV/dec under the given conditions, Figure 12 shows a contour graph for channel length and P_r/E_c using ferroelectric thickness as a parameter.

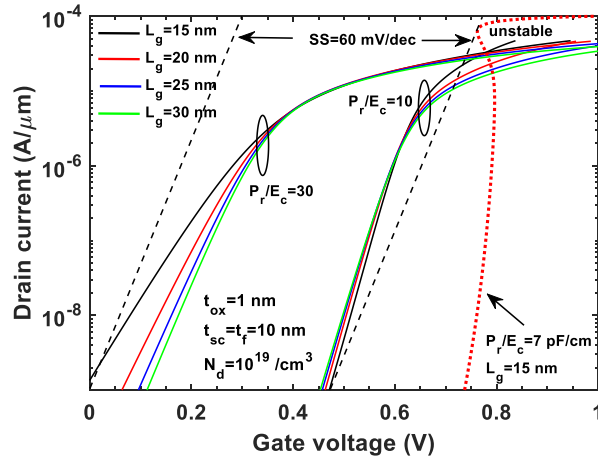


Figure 11. Subthreshold swings for the ratio of the remanent polarization P_r and coercive field E_c with a channel length as a parameter under the conditions given in the figure.

In Figure 12, the upper area of each curve indicated by a red arrow represents the $SS < 60$ mV/dec area. It can be seen that the $SS < 60$ mV/dec area increases as the ferroelectric thickness increases. In particular, it can be seen that the P_r/E_c value must also decrease as the channel length decreases to maintain $SS < 60$ mV/dec. As ferroelectric thickness decreases, the negative capacitance effect of ferroelectric also decreases, so the $SS < 60$ mV/dec area also decreases. In this way, it was found that by adjusting the values of P_r/E_c , channel length, and ferroelectric thickness, the $SS < 60$ mV/dec value could be maintained.

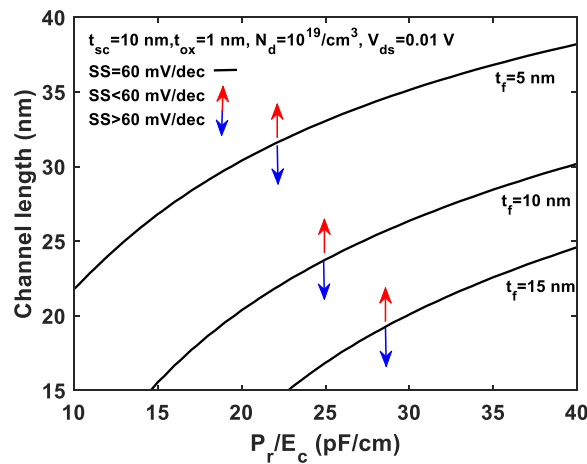


Figure 12. Contour plot for the channel length and P_r/E_c with the ferroelectric thickness as a parameter under the conditions given in the figure.

4. CONCLUSIONS

The change of SS for the junctionless double gate FeFET with MFMS structure using ferroelectric was investigated for the change of P_r and E_c of ferroelectric. The P_r and E_c were

used in the range where the unstable region does not appear in the relationship between the drain current and the gate voltage. However, it was found that the SS significantly decreased when the unstable area appeared. The change of P_r and E_c directly affected the FeFET by eventually changing the capacitance of the ferroelectric. In particular, the SS decreased as P_r decreased and E_c increased. As the memory window increased, SS decreased, and in the change of SS according to P_r and memory window, it was found that SS constantly changed according to the ratio of P_r and E_c . In conclusion, SS decreased as P_r/E_c decreased, and increased when P_r/E_c increased. The decrease in P_r/E_c eventually increases the ferroelectricity as the C_{fe} decreases in the P - E hysteresis curve, and the change in the voltage applied to the ferroelectric by the gate voltage applied to METAL2, that is, the absolute value of dV_f/dV_{gs2} increases. As a result, the SS decreased as the carrier controllability by gate voltage was improved. The smaller the channel length, the more severe the change of SS for the P_r/E_c . When the P_r/E_c ratio is relatively low, at around 10 pF/cm, the shorter the channel length, the smaller the SS. It is judged that the unstable region suddenly appears under these conditions and the SS rapidly decreases. In the future, short channel effects such as the shift of threshold voltage of FeFET and drain-induced barrier lowering (DIBL) for changes in P_r and E_c should be further analyzed.

CRedit authorship contribution statement. Hakkee Jung: Methodology, Investigation, Formal analysis.

Conflicts of interest. The author declares no conflict of interest.

REFERENCES

1. Hosseini S. A., Eskandarian A., Ghadimi A. - Three dimensional simulation of short channel effects in junction less FinFETs, *Engineering Reports* **4** (2022) e12481. DOI:10.1002/eng2.12481
2. Li X., Yuan P., Li L., Liu T., Shen C., Jiang Y., Song X., Li J., Xia C. - Promising ultra-short channel transistors based on OM2S(M=Ga,In) monolayers for high performance and low power consumption, *Nanoscale* **15** (2023) 356-364. DOI:10.1039/d2nr04840j
3. Tripathi S. L., Pathak P., Kumar A., Saxena S. - Improved Drain Current with Suppressed Short Channel Effect of p+ Pocket Double-Gate MOSFET in Sub-14 nm Technology Node, *Silicon* **14** (2022) 10881-10891. DOI:10.1007/s12633-022-01816-2
4. Mukesh S., Zhang J. - A Review of the Gate-All-Around Nanosheet FET Process Opportunities, *Electronics* **11** (2022) 3589. DOI:10.3390/electronics11213589
5. Chakrabarti H., Maity R., Baushya S., Maity N. P. - An Accurate Model of Threshold Voltage and Effect of High-k Material for Fully Depleted Graded Channel DMDG MOSFET, *Silicon* **14** (2022) 9763-9772. DOI:10.1007/s12633-021-01412-w
6. Kanith S., Vignesh N. A., Jana S., Prasad C. G., Konguvel E., Vimalnath S. - Negative Capacitance Ferroelectric FET Based on Short Channel Effect for Low Power Application, *Silicon* **14** (2022) 9569-9579. DOI:10.1007/s12633-021-01625-z
7. Kim J. Y., Choi M., Jang H. W. - Ferroelectric field effect transistors: Progress and perspective, *APL Mater.* **9**(2021) 021102. DOI:10.1063/5.0035515
8. Yu T., Lu W., Zhao Z., Si P., Zhang K. - Negative drain-induced barrier lowering and negative differential resistance effects in negative-capacitance transistors, *Microelectronics Journal* **108** (2021) 104981. DOI:10.1016/j.mejo.2020.104981
9. Alam S. U., Uddin R., Alam M. J., Raihan A., Mahtab S. S., Bhowmik S. - Mathematical Modeling and Performance Evaluation of 3D Ferroelectric Negative Capacitance FinFET,

- Modeling and Simulation in Engineering **2022** (2022) 8345513. DOI:10.1155/2022/8345513
10. Jung H. - Analysis of subthreshold swing in junctionless double gate MOSFET using stacked high-*k* gate oxide, International Journal of Electrical and Computer Engineering **11** (2021) 240-248. DOI:10.11591/ijece.v11i1.pp240-248
 11. Jung H. - Analysis of Subthreshold Swing of Junctionless Cylindrical Surrounding Gate MOSFET Using Stacked High-*k* Gate Oxide, Trans. on Electrical and Electronic Materials **23** (2022) 193-199. DOI:10.1007/s42341-022-00382-z
 12. Nadeem M., Bernardo I. D., Wang X., Fuhrer M. S., Culcer D. - Overcoming Boltzmann's Tyranny in a Transistor via the Topological Quantum Field Effect, Nano Lett. **21**(2021) 3155-3161. DOI:10.1021/acs.nanolett.1c00378
 13. Liu C., Wang Y., Sun H., Ma C., Luo Z., Wang H., Yin Y., Li X. - Positive-to-negative subthreshold swing of aMOSFET tuned by the ferroelectric switching dynamics of BiFeO₃, NPG Asia Materials **13** (2021) 77. DOI:10.1038/s41427-021-00345-5
 14. Yao J., Han X., Zhang X., Liu J., Gu M., Zhang M., Yu K., Guo Y. - Investigation on the Negative Capacitance Field Effect Transistor with Dual Ferroelectric Region, Crystals **12** (2022) 1545. DOI:10.3390/crystal12111545
 15. Cho H. W., Pujar P., Choi M., Kang S., Hong S., Park J., Baek S., Kim Y., Lee J., Kim S. - Direct growth of orthorhombic Hf_{0.5}Zr_{0.5}O₂ thin films for hysteresis-free MoS₂ negative capacitance field-effect transistors, npj 2D Materials and Applications **5** (2021) 46. DOI:10.1038/s41699-021-00229-w
 16. Gao Z., Lyu S., Lyu H. - Frequency dependence on polarization switching measurement in ferroelectric capacitors, Journal of Semiconductors **43** (2022) 014102. DOI:10.1088/1674-4926/43/1/014102
 17. Hachemi M. B., Salem B., Consonni V., Roussel H., Garraud A., Lefevre G., Labau S., Basrour S., Bsiesy A. - Study of structural and electrical properties of ferroelectric HZO films obtained by single-target sputtering, AIP Advances **11** (2021) 085004. DOI:10.1063/5.0058656
 18. Das D., Gaddam V., Jeon S. - Demonstration of High Ferroelectricity ($P_r \sim 29 \mu\text{C}/\text{cm}^2$) in Zr Rich Hf_xZr_{1-x}O₂ Films, IEEE Electron Device Letters **41** (2020)34-37. DOI:10.1109/LED.2019.2955198
 19. Das D., Buyantogtokh B., Gaddam V., Jeon S. - Influence of High-Pressure Annealing Conditions on Ferroelectric and Interfacial Properties of Zr-rich Hf_xZr_{1-x}O₂ Capacitors, IEEE Trans. Electron Devices **68** (2021) 1996-2002. DOI:10.1109/TED.2021.3061963
 20. Chen K., Chen P., Wu Y. - Proceedings of Symposium on VLSI Circuits, IEEE (2017) T84-T85. DOI:10.23919/VLSIC.2017.8008572
 21. Dang Z., Lv S., Gao Z., Chen M., Xu Y., Jiang P., Ding Y., Yuan P., Wang Y., Chen Y., Luo Q. - Improved Endurance of Hf_{0.5}Zr_{0.5}O₂-Based Ferroelectric Capacitor Through Optimizing the Ti-N Ratio in TiN Electrode, IEEE Electron Device Letters **43** (2022) 561-564. DOI:10.1109/LED.2022.3153063
 22. Yuan P., Wang B., Yang Y., Lv S., Wang Y., Xu Y., Jiang P., Chen Y., Dang Z., Ding Y., Gong T., Luo Q. - Enhanced Remanent Polarization ($30 \mu\text{C}/\text{cm}^2$) and Retention of Ferroelectric Hf_{0.5}Zr_{0.5}O₂ by NH₃ Plasma Treatment, IEEE Electron Device Letters **43** (2022) 1045-1048. DOI:10.1109/LED.2022.3178867

23. Lin Y., Rayner G. B., Cardenas J., Franklin A. D. - Short-channel robustness from negative capacitance in 2D NC-FETs, *Appl. Phys. Lett.* **118** (2021) 101903. DOI:10.1063/5.0030555
24. Tu L., Wang X., Wang J., Meng X., Chu J. - Ferroelectric Negative Capacitance Field Effect Transistors, *Adv. Electron. Mater.* **4** (2018) 1800231. DOI:10.1002/aelm.201800231
25. Kashir A., Kim H., Oh S., Hwang H. - Large Remanent Polarization in a Wake-Up Free $\text{Hf}_{0.5}\text{Zr}_{0.5}\text{O}_2$ Ferroelectric Film through Bulk and Interface Engineering, *ACS Applied Electronic Materials* **3** (2021) 629-638. DOI:10.1021/acsaelm.0c00671
26. Asapu S., Pagaduan J. N., Zhuo Y., Moon T., Midya R., Gao D., Lee J., Wu Q., Barnell M., Gangguli S., Katsumata R., Chen Y., Xia Q., Yang J. J. - Large remanent polarization and great reliability characteristics in W/HZO/W ferroelectric capacitors., *Frontiers in Materials* **9** (2022) 969188. DOI:10.3389/fmats.2022.969188
27. Khakimov R. R., Chernikova A. G., Koroleva A. A., Markeev A. M. - On the Reliability of HZO-Based Ferroelectric Capacitors: The Cases of Ru and TiN Electrodes, *Nanomaterials* **12** (2022) 3059. DOI:10.3390/nano12173059
28. Okuno J., Kunihiro T., Konishi K., Maemura H., Shuto Y., Sugaya F., Materano M., Ali T., Kuehnel K., Seidel K., Schroeder U., Mikolajick T., Tsukamoto M., Umebayashi T. - Proceedings of Symposium on VLSI Technology, *IEEE* (2020) 1-2. DOI:10.1109/VLSITechnology18217.2020.9265063
29. Francois T., Grenouillet L., Coignus J., Blaise P., Carabasse C., Vaxelaire N., Magis T., Aussenac F., Loup V., Pellissier C., Slesazek S., Havel V., Richter C., Makosiej A., Giraud B., Breyer E. T., Materano M., Chiquet P., Bocquet M., Nowak E., Schroeder U., Gaillard F. - Proceedings of 2019 IEEE International Electron Devices Meeting (IEDM), *IEEE* (2019) IEDM19-362-365. DOI:10.1109/IEDM19573.2019.8993485
30. Liang Y., Wu J., Teng C., Ko H., Luc Q., Su C., Chang E., Lin C. - Demonstration of Highly Robust 5nm $\text{Hf}_{0.5}\text{Zr}_{0.5}\text{O}_2$ Ultra-Thin Ferroelectric Capacitor by Improving Interface Quality, *IEEE Electron Device Letters* **42** (2021) 1299-1302. DOI:10.1109/LED.2021.3102604
31. Ding Z., Hu G., Gu J., Liu R., Wang L., Tang T. - An analytical model for channel potential and subthreshold swing of the symmetric and asymmetric double-gate MOSFETs, *Microelectronics Journal* **42** (2011) 515-519. DOI:10.1016/j.mejo.2010.11.002
32. Jung H. - Analytical Model of Subthreshold Swing for Junctionless Double Gate MOSFET using Ferroelectric Negative Capacitance Effect, *IIUM Engineering Journal* **24** (2023) 75-87. DOI:10.31436/iiumej.v24i1.2508
33. Wang K., Haung Q., Su C., Chen L., Yang M., Haung R. - Impacts of Ferroelectric Parameters on the Electrical Characteristics of Fefet for Low-Power Logic and Memory Applications, *Proceedings of 2021 China Semiconductor Technology International Conference (CSTIC), IEEE* (2021) 1-3. DOI:10.1109/CSTIC52283.2021.9461542
34. Boscke T. S., Muller J., Brauhaus D., Schroder U., Bottger U. - Ferroelectricity in hafnium oxide thin films, *Applied Physics Letters* **99** (2011) 102903. DOI:10.1063/1.3634052
35. Kim H., Hong D., Yoo J., Lee H. - Effect of Process Temperature on Density and Electrical Characteristics of $\text{Hf}_{0.5}\text{Zr}_{0.5}\text{O}_2$, Thin Films Prepared by Plasma-Enhanced Atomic layer Deposition, *Nanomaterials* **12** (2022) 548. DOI:10.3390/nano120330548